Original

Xi, H.; Larouche, P.; Tang, S.; Michel, C.:
Characterization and variability of particle size distributions in Hudson Bay, Canada.
In: Journal of Geophysical Research : Oceans. Vol. 119 (2014) 6, 3392 - 3406.
First published online by AGU: 14.05.2014

http://dx.doi.org/10.1002/2013JC009542

AGU PUBLICATIONS

JGR

Journal of Geophysical Research: Oceans

RESEARCH ARTICLE

10.1002/2013JC009542

Characterization and variability of particle size distributions in Hudson Bay, Canada

Hongyan Xi[1,2], Pierre Larouche[1], Shilin Tang[3,4], and Christine Michel[3]

[1]Maurice Lamontagne Institute, Fisheries and Oceans Canada, Mont-Joli, Québec, Canada, [2]Institute of Coastal Research, Helmholtz-Zentrum Geesthacht, Geesthacht, Germany, [3]Freshwater Institute, Fisheries and Oceans Canada, Winnipeg, Manitoba, Canada, [4]South China Sea Institute of Oceanology, Chinese Academy of Sciences, Guangzhou, People's Republic of China

Key Points:
- Significant regional and vertical variability in the PSD
- A strong association of larger particles with the base of mixed layer observed
- Potential of remote estimate of PSCs from PSD in offshore waters

Correspondence to:
H. Xi,
hongyan.xi@hzg.de

Citation:
Xi, H., P. Larouche, S. Tang, and C. Michel (2014), Characterization and variability of particle size distributions in Hudson Bay, Canada, *J. Geophys. Res. Oceans*, *119*, 3392–3406, doi:10.1002/2013JC009542.

Received 24 OCT 2013
Accepted 12 MAY 2014
Accepted article online 14 MAY 2014
Published online 5 JUN 2014

Abstract Particle size distribution (PSD) plays a significant role in many aspects of aquatic ecosystems, including phytoplankton dynamics, sediment fluxes, and optical scattering from particulates. As of yet, little is known on the variability of particle size distribution in marine ecosystems. In this study, we investigated the PSD properties and variability in Hudson Bay based on measurements from a laser diffractometer (LISST-100X Type-B) in concert with biogeochemical parameters collected during summer 2010. Results show that most power-law fitted PSD slopes ranged from 2.5 to 4.5, covering nearly the entire range observed for natural waters. Offshore waters showed a predominance of smaller particles while near the coast, the effect of riverine inputs on PSD were apparent. Particulate inorganic matter contributed more to total suspended matter in coastal waters leading to lower PSD slopes than offshore. The depth distribution of PSD slopes shows that larger particles were associated with the pycnocline. Below the pycnocline, smaller particles dominated the spectra. A comparison between a PSD slope-based method to derive phytoplankton size class (PSC) and pigment-based derived PSC showed the two methods agreed relatively well. This study provides valuable baseline information on particle size properties and phytoplankton composition estimates in a sub-arctic environment subject to rapid environmental change.

1. Introduction

Particle size in marine waters is influenced by many processes including biological growth, flocculation, aggregation, disaggregation, and sedimentation. These different processes dominate at different size scales. Particle size distribution (PSD), i.e., the relationship between particle sizes and their concentrations, has been widely used to characterize marine particles [*Bader*, 1970]. PSD provides important information about pelagic ocean ecosystem structure and function and is therefore of particular significance in diverse fields in oceanography, from sedimentology to biology. An understanding of PSD is required to assess the composition of particle assemblages, plankton populations, and phytoplankton functional types [*Falkowski et al.*, 1998; *Neukermans et al.*, 2012; *Karp-Boss*, 2007; *Kostadinov et al.*, 2010, 2012], as well as to characterize sediment fluxes, particle resuspension, and sinking rates [*Mikkelsen and Pejrup*, 2001; *Ahn*, 2012]. PSD also plays a strong role in the propagation of light in the water, especially in spectral attenuation and scattering [*Boss and Pegau*, 2001; *Boss et al.*, 2001a, 2001b; *Twardowski et al.*, 2001]. In bio-optical applications, the optical methods provide an estimate of the change in the average size of particles. Assuming that the power-law distribution is a good representation of the PSD, the PSD slope is often theoretically related to the spectral slope of the particulate beam attenuation coefficient, $c_p(\lambda)$, which also exhibits an inverse power-law dependence on wavelength [*Morel*, 1973; *Boss et al.*, 2001a, 2001b; *Twardowski et al.*, 2001; *Sullivan et al.*, 2005]. The same is true of the particulate backscattering coefficient, $b_{bp}(\lambda)$, though the backscattering is largely attributed to different size range and particles [*Stramski and Kiefer*, 1991; *Stramski et al.*, 2001; *Dall'Olmo et al.*, 2009]. However, it should be noted that b_{bp} does not usually exhibit an inverse power-law dependence in the visible range due to the effect of absorption peaks. A better understanding of bio-optical properties improves the application technologies to relate ocean color and PSD to optical properties. In remote-sensing applications, the $b_{bp}(\lambda)$ slope has been used to describe and quantify the PSD slope and the particle number density $N'(D)$, as in recent models [*Loisel et al.*, 2006; *Kostadinov et al.*, 2009]. The relationship of the $b_{bp}(\lambda)$ slope to the PSD has, however, remained ambiguous [*Kostadinov et al.*, 2012], and this is exacerbated in optically complex waters [*Aurin et al.*, 2010]. Given that the PSD provides important

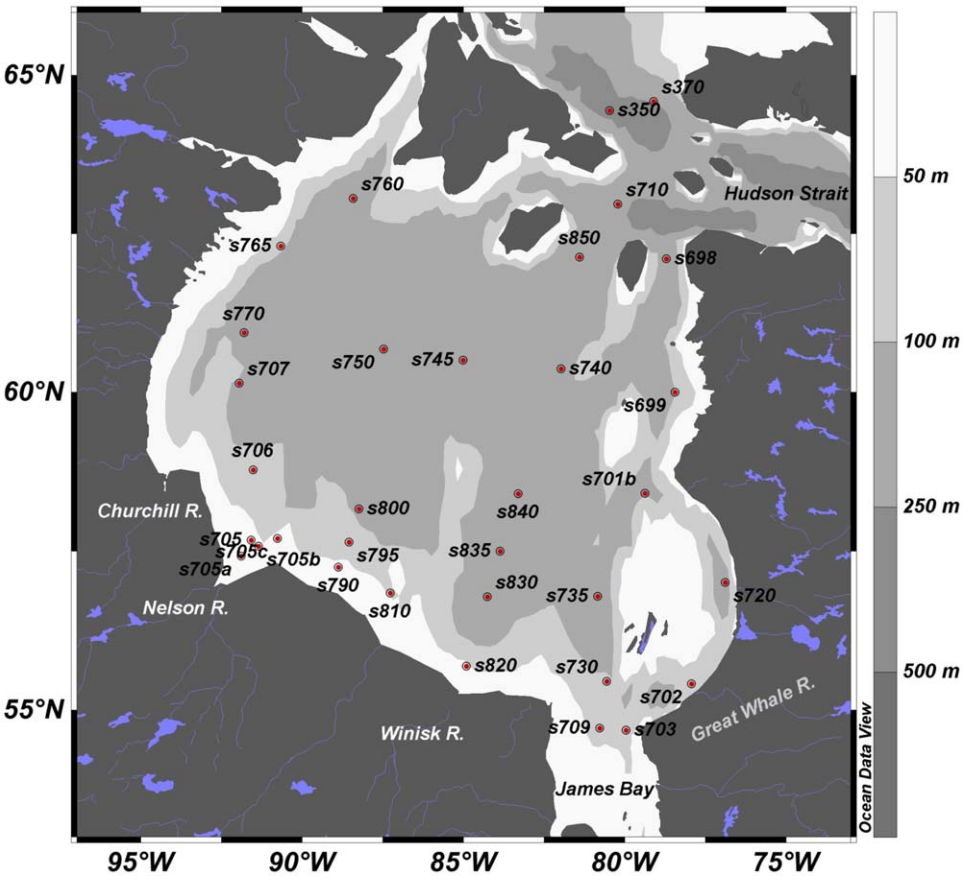

Figure 1. Study area and stations in Hudson Bay during the ArcticNet 2010 expedition.

information on the dominant phytoplankton size classes (PSCs) [*Falkowski et al*., 1998, 2003; *Hood et al*., 2006], it is also possible to assess PSCs from PSD derived from remote sensing. Assuming that the open ocean particulate assemblage is biogenic, *Kostadinov et al*. [2010] assessed the global distribution and dynamics of PSCs using a new method to retrieve the parameters of a power-law PSD from ocean color remote sensing data. This opens up the possibility of using water-leaving radiance-derived PSD from satellite data to estimate phytoplankton functional types.

The regional variability of PSD slopes has been addressed in a few recent studies. Large PSD slopes and low particle concentrations are typically found in open waters while smaller slopes and higher concentrations are found in estuarine waters and river plumes [*Buonassissi and Dierssen*, 2010]. Significant spatial and temporal variability in both concentration and shape of the PSD was demonstrated in situ [*Reynolds et al*., 2010]. *Karageorgis et al*. [2012] also reported significant spatial and seasonal variability in particulate matter abundance (or concentration) and size distributions in the Eastern Mediterranean Sea. The objective of this study is to characterize PSD spatial variability, at both horizontal and vertical scales, and examine relationships with phytoplankton assemblages in a large sub-arctic sea, Hudson Bay, Canada.

2. Material and Methods

2.1. Study Area and Sampling

The data used in this study were collected at 33 stations during the summer 2010 ArcticNet expedition (between 9 and 31 July) in Hudson Bay (Figure 1), a large sub-arctic inland sea with complex optical properties due to a large influx of freshwater mostly in its southern portion [*Xi et al*., 2013]. Water samples for pigment and particle concentrations were collected at discrete depths, including the surface, depth of deep chlorophyll maximum (DCM), and other optical depths. Surface water samples were collected using a clean

bucket while samples at other depths were collected using a rosette equipped with 12 L Niskin-type bottles. An optical profiling package made of a variety of instruments was used to measure various optical, biogeochemical, and physical water properties. These instruments were a Sequoia LISST-100X to measure the size spectra of particles up to 250 μm, a Seabird SBE49 CTD to measure the vertical physical structure of the water column and a WetStar fluorometer to measure chlorophyll fluorescence (Chl fluorescence). The profiling package was slowly (0.2 m s^{-1}) lowered in the water column down to a depth of 100 m. Only downcast measurements have been used in this study to minimize interference from the instrument cage.

2.2. PSD Measurements

The PSD were estimated from field measurements of the volume scattering function performed using a LISST-100X Type-B particle size analyzer (Sequoia, Inc.). An additional photodiode detector records transmitted light, from which the beam attenuation coefficient of particles at 670 nm, $c_p(670)$, can be calculated. There are 32 size ranges logarithmically placed from 1.25 to 250 μm in diameter (the upper size in each bin is 1.18 times the lower), with the width of individual size classes varying from 0.2 to 35 μm. Scattered light in the near forward angles is measured on concentric detector rings and inversion modeling based on Mie theory yields the particle volume concentration, $V(\mathrm{D})$, in the 32 size classes [*Agrawal and Pottsmith*, 2000]. D is the geometric average of the two boundaries of each class bin and is often represented as a volume-equivalent sphere due to the unknown particle shape. In order to measure only the scattered light contributed by the particles, the background scattering measurement of LISST was acquired beforehand. $V(\mathrm{D})$ was then calculated using the manufacturer provided software LISST-SOP and calibration [*LISST-100X Particle Size Analyzer*, 2013]. The particle number distribution, $N(\mathrm{D})$, was calculated from the equation:

$$N(\mathrm{D}) = 6V(\mathrm{D})/\pi \mathrm{D}^3. \tag{1}$$

The PSD can be defined as the average number of particles within a given size class of width $\Delta\mathrm{D}$ for a unit volume of suspension [e.g., *Jonasz and Fournier*, 2007; *Reynolds et al*., 2010] and is expressed as

$$N'(\mathrm{D}) = N(\mathrm{D})/\Delta\mathrm{D}. \tag{2}$$

Accordingly, the differential volume concentration of particles per unit size, $V'(\mathrm{D})$, is expressed as $V'(\mathrm{D}) = V(\mathrm{D})/\Delta\mathrm{D}$.

Mikkelsen et al. [2008] showed that density differences observed at pycnoclines can induce light scattering—schlieren—that artificially increases the proportion of large particles in the PSD and may pose problems for the interpretation of results. One way to detect schlieren is to compare beam attenuation (c_p) calculated from LISST measurements to c_p measured using a wider acceptance angle instrument. Fortunately, the ship's rosette was equipped with a WETLabs C-Star transmissometer allowing the comparison of c_p between both instruments. Even though the measurements were not simultaneous, the comparison between both casts showed that coastal stations were potentially affected by schlieren near the pycnocline. Considering this, we filtered the vertical PSD profiles by eliminating all measurements for which LISST c_p was above a threshold value of 0.75 m^{-1} down to the depth of 40 m as high LISST c_p values below that depth were similar to C-Star c_p. That threshold was selected by plotting LISST c_p against C-Star c_p. Schlieren affected PSD were easily identified as outliers with large LISST c_p at low C-Star c_p. Of the whole PSD measured, only 5% were found contaminated and removed from further analysis.

There are several mathematical descriptions of the PSD proposed for marine systems including power-law model (or Junge distribution), Gaussian or lognormal distributions, and the gamma function [*Bader*, 1970; *Jonasz*, 1983; *Risovic*, 1993]. Among these models, the power law is the most frequently used for optical and ecological purposes [e.g., *Jonasz*, 1983; *Bricaud et al*., 1981; *Stramski and Kiefer*, 1991] and has been theoretically justified in many studies [e.g., *Sheldon et al*., 1972; *Platt and Denman*, 1978; *Kiefer and Berwald*, 1992]. Though the other models are able to describe the PSD spectra more precisely than the power-law model, it is difficult to directly relate the derived PSD characteristics from these models with optical and biogeochemical analyses. This is why we choose to use the power-law model even if it is imperfect. The following power-law function can be fitted to the PSD data over a selected size range

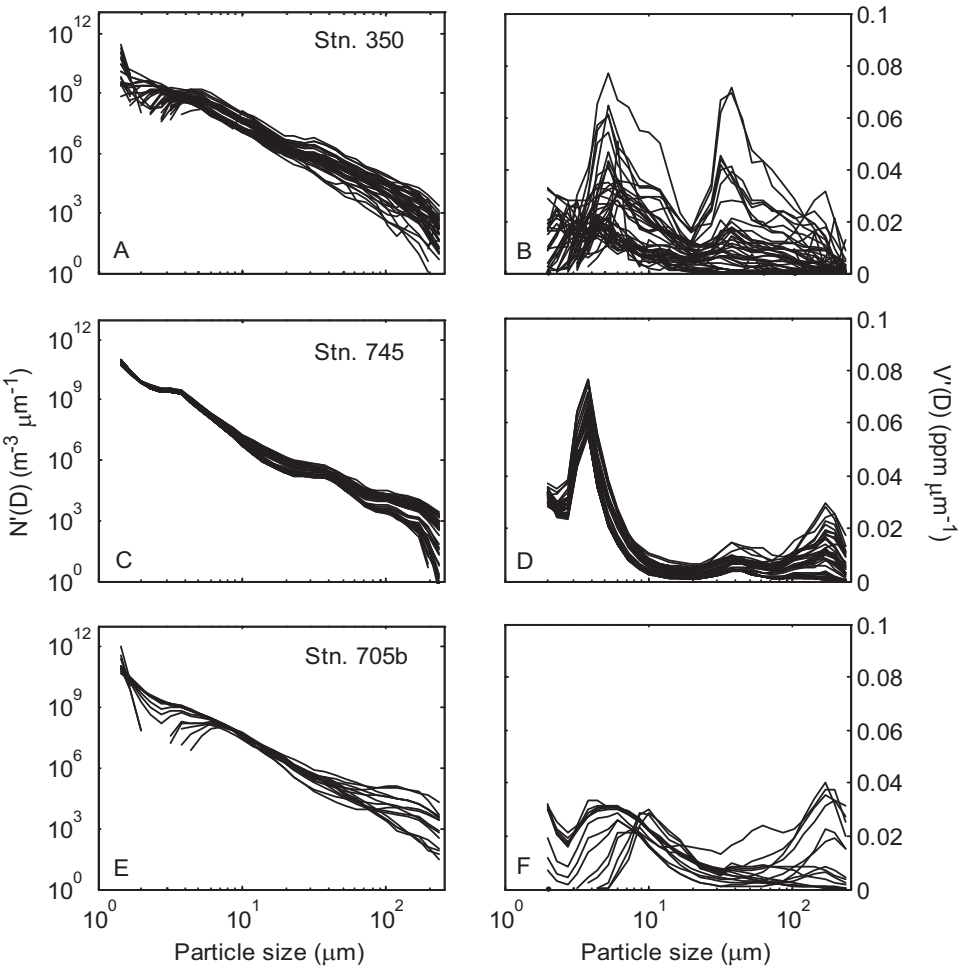

Figure 2. (a, c, e) Particle number density $N'(D)$ and (b, d, f) volume concentration density $V'(D)$ measured with the LISST at three representative stations for various depths. (top) Stn. 350 (0–100 m); (middle) Stn. 745 (0–100 m); and (bottom) Stn. 705b (0–35 m).

$$N'(D) = N'(D_o)\left(\frac{D}{D_o}\right)^{-\xi}, \tag{3}$$

where D_o is a reference diameter, the nondimensional ξ is the PSD slope (or Junge exponent), and $N'(D_o)$ is the differential number concentration at D_o (units of m^{-3} μm^{-1}). Calculations were done using least squares minimization on the log-transformed data of each distribution as performed in previous studies [*Vidondo et al*., 1997; *Reynolds et al*., 2010; *Buonassissi and Dierssen*, 2010]. The relative concentration of small to large particles was estimated by the PSD slope calculated by the power-law model.

Considering that the PSD slope is not only sensitive to the fitting method but also to the range of particle size used for its calculation, deviations from the power-law model can lead to differences in the estimated PSD parameters. The LISST-100X instrument has been shown to be sensitive to the presence of particles in suspension that are finer than the measurement range of the optics [*Agrawal and Traykovski*, 2001; *Agrawal et al*., 2008; *Buonassissi and Dierssen*, 2010] leading to a rising tail at small size class. *Andrews et al*. [2010] attribute the rising tail to improper choice of refractive index for small particles. This contamination is evident in our data set (Figure 2) mostly for size classes less than 6 μm. Previous studies have shown that LISST PSD measured over larger size classes (>6 μm) are generally consistent with measurements from other instruments [*Reynolds et al*., 2010; *Buonassissi and Dierssen*, 2010].

Considering this, the PSD slope ξ was calculated using equation (3) within the size range of 6.14–196 μm. This range minimizes the effect of the tail at smaller size range and the very low values at the largest size classes on the slope calculation. Null data at some small size classes due to the tail were removed. The

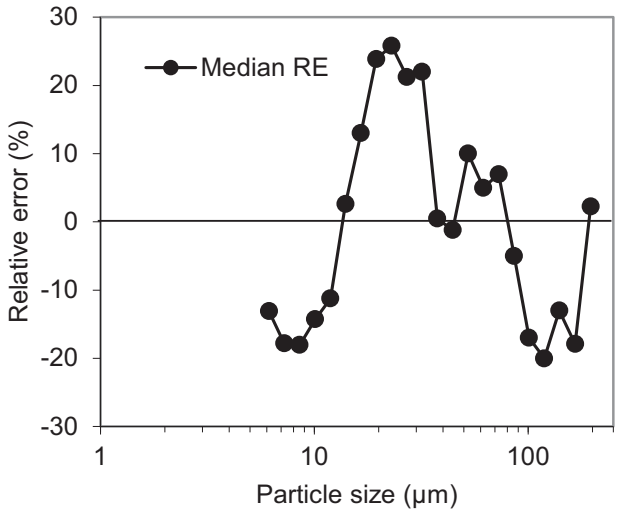

Figure 3. Median values of the relative error (RE, %) against particle sizes to show the bias of the modeled *N*(D) compared to the observed *N*(D).

size class 37.6 μm was selected as the reference particle size D_o because it is the midpoint of the logarithmic size range. The linear least squares fit to the log-transformed data provided good regression statistics with determination coefficient R^2 between 0.88 and 0.99 and significant *p* value <0.01 for all sampled stations. In addition to the regression statistics of the power-law model, the residuals were also calculated to verify whether significant deviations occurred between the observed and modeled data. Relative errors (RE, %) were calculated in each size class for all the PSD in the data set, $RE = [N(D)_{mod} - N(D)_{obs}]/N(D)_{obs} \times 100\%$, where $N(D)_{mod}$ and $N(D)_{obs}$ represent the modeled and observed particle number concentration, respectively. Figure 3 shows that the median values of the relative errors as a function of particle sizes ranging between 6.14 and 196 μm were within ±30%. The particle number concentrations were underestimated in the ranges of 6–10 μm and 80–200 μm while overestimated in the 20–30 μm and 50–70 μm size ranges. This error pattern was tightly associated to the distinctive peaks in the PSD (see Figure 2), resulting from the predominance of particles at certain sizes that are not captured by the power-law model [*Reynolds et al*., 2010]. Results from the regression statistics and residual analysis were consistent with previous results on the power-law performance [*Reynolds et al*., 2010; *Buonassissi and Dierssen*, 2010], suggesting that though having limitations in capturing spectral complexities of the PSD, the power-law model proved to be a reasonable approximation and can easily be used to analyze the properties and variability of the PSD in relation to optical and biogeochemical parameters in Hudson Bay. After calculation, the PSD data at each vertical profile were median-binned to 1 m intervals. Note that near the surface LISST measurements usually tend to be interfered by ambient light conditions in oligotrophic environments [*Andrews et al*., 2011]. In our study, the binned PSD data were checked from station to station and those showing abnormal shapes at the very surface (0–2 m) were discarded as in previous studies [*Agrawal*, 2005; *Mikkelsen et al*., 2008].

2.3. Particle and Pigment Measurements

Samples for total suspended matter (TSM) and chlorophyll-*a* (Chl-*a*) concentration were collected at discrete depths including the surface, the DCM depth, and other depths (such as 10 and 20 m, 15% and 30% light penetrating depths. Note that not all these depths were sampled at each station). For TSM measurement, 0.5–3 L of sea water was filtered under low pressure onto preweighed 25 mm glass fiber filters (Whatman, GF/F). The filters were rinsed with Milli-Q water and kept frozen at −20°C until dried at 100°C for at least 3 h. The filters were weighed to measure the total suspended matter (TSM) concentration and combusted at 550°C for 1 h and reweighed to measure the particulate inorganic matter (PIM) concentration. The particulate organic matter (POM) concentration was obtained by subtracting PIM from TSM. High-performance liquid chromatography (HPLC) was used to determine the liposoluble pigment concentrations on samples filtered onto 25 mm Whatman GF/F filters under low pressure. The samples were processed at the Horn Point Laboratory (see *Van Heukelem and Thomas* [2005] for a complete description of the methodology). HPLC Chl-*a* concentration in this study is defined as the sum of chlorophyll-*a* allomers and epimers, divinyl chlorophyll-*a*, and chlorophyllids-*a*. Size-fractionated chlorophyll measurements were also done using the fluorescence method [*Yentsch and Menzel*, 1963] for the following size classes (<5 μm, 5–20 μm, and >20 μm). In addition, chlorophyll fluorescence vertical profiles from WetStar fluorometer were also obtained. The fluorescence was binned into 1 m intervals.

Table 1. Linear Correlation Coefficients Between Optical Measurements and Biogeochemical Parameters[a]

	HPLC Chl-*a*	Fluo. Chl-*a*	TSM	PIM	POM
Fluo. Chl-*a*	0.95*				
TSM	0.60*	0.59*			
PIM	0.63*	0.65*	0.93*		
POM	0.18	0.20	0.65*	0.35	
LISST $c_p(670)$	0.33	0.43	0.56*	0.52*	0.46*

[a]Variable symbols and units are as follows: HPLC Chl-*a*, chlorophyll *a* concentrations measured with HPLC in mg m^{-3}; Fluo. Chl-*a*, chlorophyll-*a* concentrations measured by fluorescence method; TSM, total suspended matter concentrations in g m^{-3}; PIM, particulate inorganic matter concentrations in g m^{-3}; POM, particulate organic matter concentrations in g m^{-3}; LISST $c_p(670)$, particulate beam attenuation coefficients at 670 nm measured with LISST in m^{-1}. Significant correlation ($p < 0.01$) is marked with an asterisk.

2.4. Phytoplankton Size Class (PSC)

Two methods were used to determine the PSCs in our study. First, HPLC data were used to estimate the contribution of picoplankton (BP_{pico}: <2 μm), nanoplankton (BP_{nano}: 2–20 μm), and microplankton (BP_{micro}: >20 μm) to total biomass based on pigment composition by the HPLC pigment-derived classes methods [*Vidussi et al*., 2001; *Uitz et al*., 2006]. The second method is based on the calculation of the PSD slope ξ from LISST data. Here we assume that PSD obeys the power-law model and the PSD slopes also apply to particles smaller than 6 μm. LISST slope-based PSCs are defined as the percent contribution of pico (0.2–2 μm), nano (2–20 μm), and microplankton sized (20–200 μm) particles to the total volume concentration in the range of 0.2–200 μm. The estimates of ξ were used to calculate the LISST slope-based PSCs after *Kostadinov et al*. [2009, 2010] using the following equation:

$$\mathrm{BP\_PSC} = \frac{D_{PSCmax}^{4-\xi} - D_{PSCmin}^{4-\xi}}{D_{max}^{4-\xi} - D_{min}^{4-\xi}}, \tag{4}$$

where D_{PSCmax} and D_{PSCmin} are the size limits of the PSC size class of interest, and $D_{min} = 0.2$ μm and $D_{max} = 200$ μm are the lower and upper limits of the size range considered.

Relating the PSD to the PSCs assumes that the particle assemblage is of biogenic origin and that living phytoplankton represents a constant proportion of all particles by volume at all considered size classes [*Kostadinov et al*., 2010, 2012]. This assumption is likely to be violated in coastal areas or in areas dominated by inorganic particles. Significant deviations from the simple first-order power-law model may also be expected, especially in coastal areas [*Reynolds et al*., 2010].

2.5. Uncertainties in Measurements and Intercomparisons

Discrete measurements of TSM and HPLC Chl-*a* were done on individual samples (no duplicates or triplicates). However, blank samples (1–2 L of Milli-Q water processed as a sample) were done regularly to evaluate the accuracy of the measurement/analysis process. The mean coefficient of variation (CV) of TSM was 15%, while the mean CV of HPLC Chl-*a* was small (0.49%). The linear correlation coefficients between the different biogeochemical parameters are given in Table 1. Results show that TSM is significantly correlated with all other variables. The same variable but measured with different techniques (i.e., HPLC Chl-*a* versus Fluo. Chl-*a*) shows satisfactory correlations as well. The Fluo. Chl-*a* versus HPLC Chl-*a* are in good agreement but the Fluo. Chl-*a* is higher than HPLC Chl-*a* (Notation section, $R = 0.95$, $p < 0.001$, slope = 1.98, figure not shown). Such a high ratio has also been found in other polar environments [*Mustapha et al*., 2012; *Marrari et al*., 2006; *Darecki et al*., 2005]. HPLC Chl-*a* values are used to investigate the relationship between Chl-*a* and PSD slopes and its regional variability.

3. Results and Discussion

3.1. Regional Variability of the Surface PSD

The surface PSDs were obtained by averaging PSDs from 2 to 5 m in order to represent the first optical depth in Hudson Bay. The very surface data (depth less than 2 m) were discarded because some stations showed contamination by ambient light [*Andrews et al*., 2011]. Note that the surface mixed layer depth (MLD) was calculated for each individual CTD profile. The mean MLD was 14 m while the mean 30% light penetrating depth was 10 m [*Xi et al*., 2013], ensuring that the surface values of PSD and biogeochemical parameters can adequately represent the first optical depth. The surface PSD slopes ranged from 2.84 to 4.46 with a mean value of 3.63 ± 0.40, covering nearly the entire range observed for natural waters

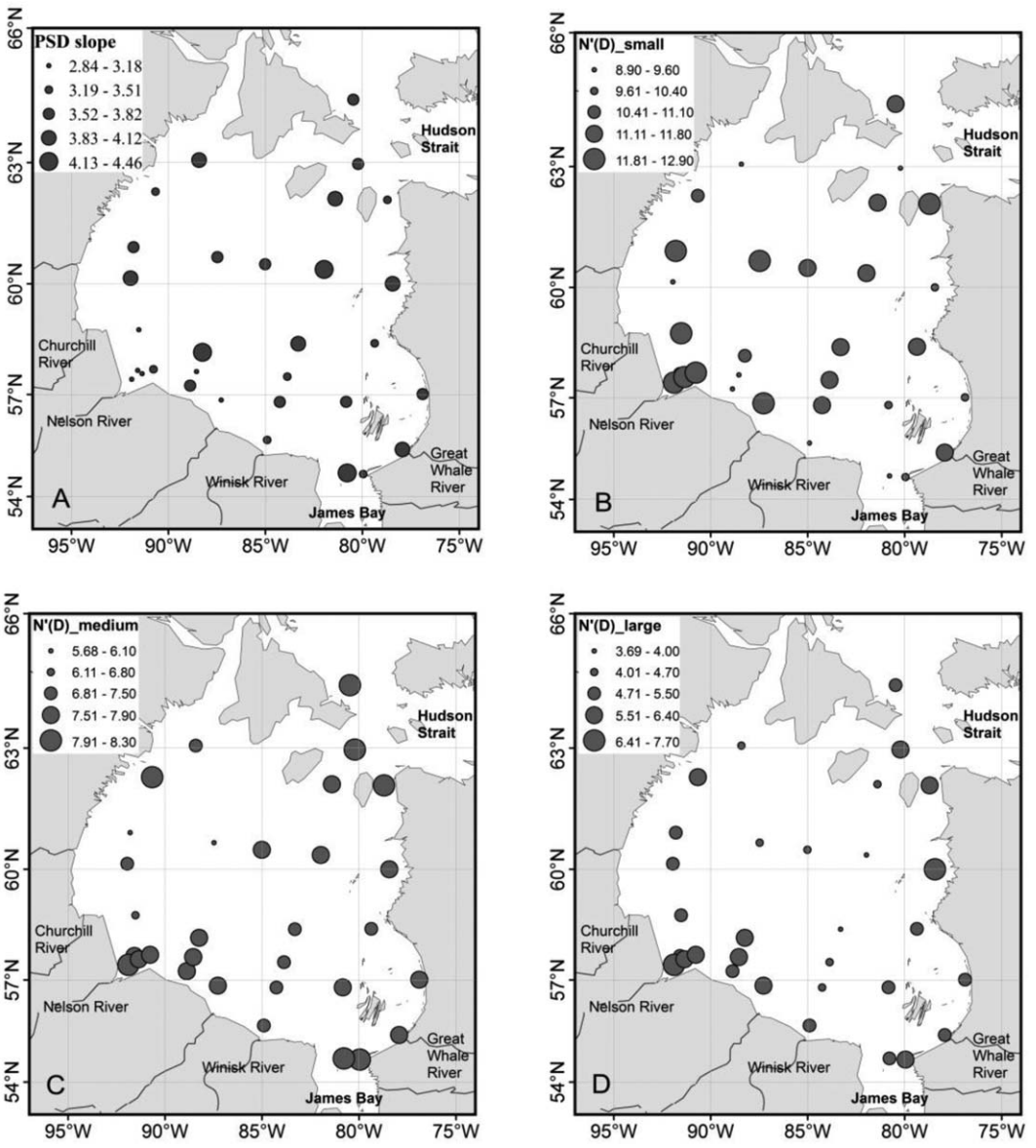

Figure 4. (a) Spatial distribution of the power-law fitted surface PSD slope, and total particle number density for (b) small size class (<10 μm), (c) medium size class (10–50 μm), and (d) large size class (>50 μm) (unit: m^{-3} μm^{-1}). Note that 10-based logarithm was performed and the corresponding exponents are shown in Figures 4b–4d.

[*Jonasz*, 1983; *Loisel et al*., 2006; *Jonasz and Fournier*, 2007; *Boss et al*., 2001a; *Reynolds et al*., 2010; *Kostadinov et al*., 2012; *Buonassissi and Dierssen*, 2010]. Steeper slopes were indicative of the higher relative abundance of the smaller particles [*Bader*, 1970]. Figure 4a shows that, in general, the steepest slopes ($\xi \geq 4$) occurred in the oligotrophic offshore stations, while the shallowest slopes ($\xi \leq 3$) were found in the Nelson River estuary, where freshwater inputs are substantial and the particle assemblages are more complex. Figures 4b–4d show the spatial distribution of the total PSD particle number concentrations for three size classes (small: <10 μm, medium: 10–50 μm, and large: >50 μm). There was no significant regional variation in total particle numbers $N'(D)$ for the small size class except for several stations with very low values due to the LISST failure at finer size classes. For both medium and large size classes, total $N'(D)$ was higher in the coastal waters than offshore waters. This phenomenon is significant particularly for the large size class with approximately 4 orders of magnitude between the maximum at Stn. 705a and minimum at Stn. 740. The Nelson River estuary showed the highest particle load, likely due to the terrigenous material exported by the river.

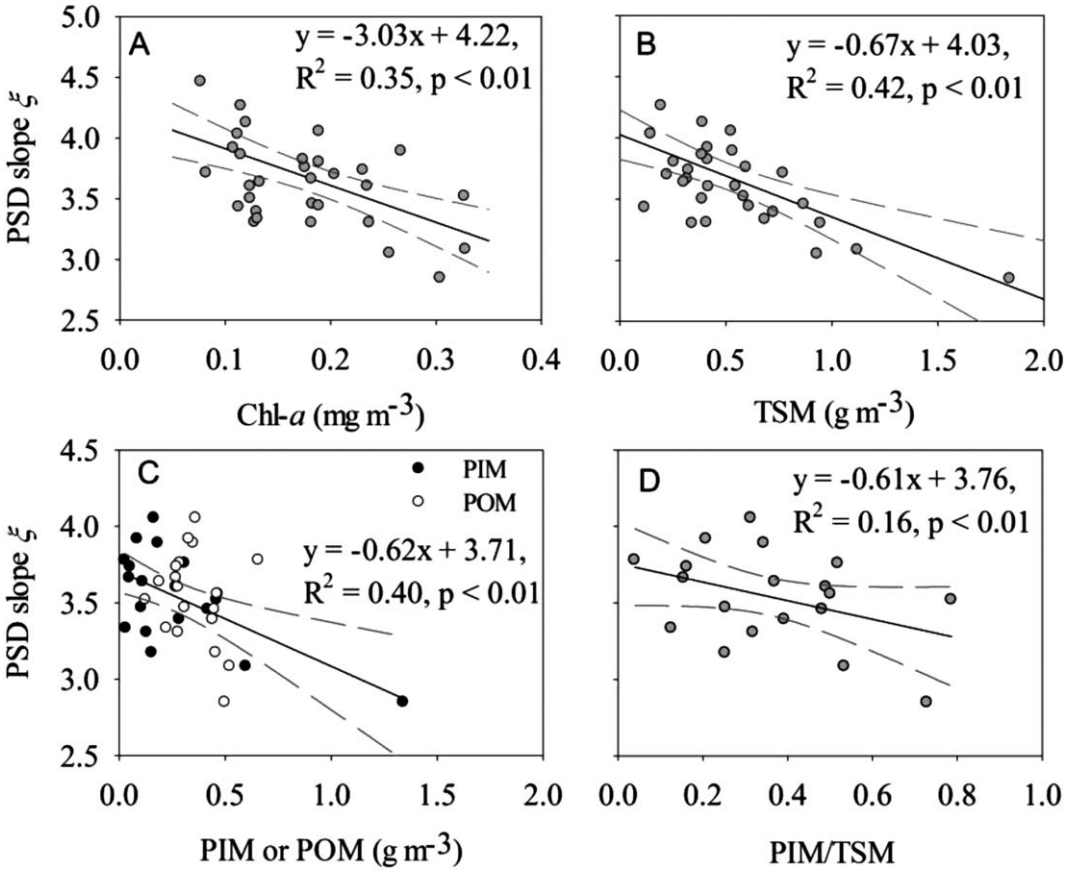

Figure 5. Scatterplots of (a) PSD slope versus Chl-*a*, (b) PSD slope versus TSM, (c) PSD slope versus PIM or POM, and (d) PSD slope versus PIM/TSM ratio with linear regression lines (solid) and 95% confidence intervals (gray dashed lines). In Figure 5c, regression line is plotted between PIM and the PSD slope.

The relationships between PSD slopes and biogeochemical parameters were also investigated. Given that Chl-*a* concentration can be partially related to phytoplankton cell sizes [*Bricaud et al*., 2004] and that TSM concentration also covaries with particle assemblages, *Sullivan et al*. [2005] proposed that higher (lower) Chl-*a* and TSM would more likely exist in regions with larger (smaller) particles and lower (higher) PSD slopes. Surface HPLC Chl-*a* ranged from 0.07 to 0.33 mg m^{-3} and TSM ranged from 0.12 to 1.84 g m^{-3}, indicative of oligotrophic conditions and low phytoplankton biomass during the summer sampling period. Figure 5 shows that, for the surface layer, the PSD slope values were inversely related to Chl-*a* and TSM concentrations. Particulate inorganic matter (PIM) also showed an inverse relationship with PSD slopes. However, no correlation was found between PSD slopes and particulate organic matter (POM). The latter can be explained by the weak correlation between POM and Chl-*a*, indicating that for many stations, phytoplankton was not the main contributor to POM [*Xi et al*., 2013]. The proportion of PIM to TSM was also well correlated with the PSD slope, showing that PIM contributes more to TSM in coastal waters where the PSD slopes are lower. Determining such relationships helps to understand the role of phytoplankton in ecosystem structure, particle size distribution, and particulate composition.

3.2. Vertical Variability of the PSD

Overall, more than 98% of ξ values were located in the (2.5–4.5) range with a mean value of 3.66 and SD of 0.37. ξ values were divided into three groups roughly representing the upper layer (0–10 m), middle layer (10–30 m), and the deep layer (30–100 m). Figure 6 shows the histograms of ξ distribution for the three layers for all stations. The mean ξ values were 3.64, 3.50, and 3.76 for the upper, the middle, and the deep layer, respectively. The distribution of ξ values in the surface layer was slightly wider (SD = 0.43) as this layer is directly impacted by river runoff that generates small ξ values (Figure 4). The slope distribution was slightly more compact at intermediate depths (SD = 0.37), with some regions showing spectra dominated

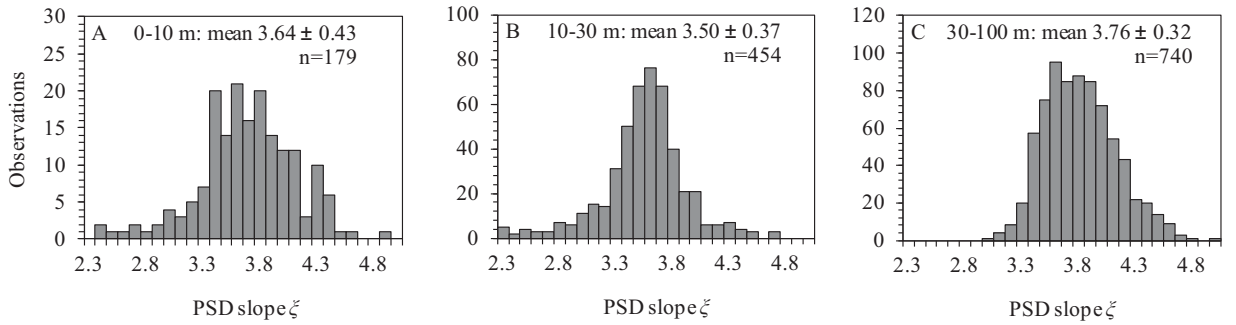

Figure 6. Histogram of the modeled PSD slope ξ at (a) upper (0–10 m) layer, (b) middle (10–30 m) layer, and (c) deep (30–100 m) layer. Mean values and standard deviations (SD) are provided.

by the presence of large particles (small ξ), such as Stn. 705a at the Nelson River estuary and Stn. −709 at the entrance of James Bay, with the smallest ξ values (2.21 and 2.24) measured in Hudson Bay. For the deeper layer (30–100 m), the slope values distribution was even narrower (SD = 0.32) with no trace of large particles dominated spectra and a clear dominance of smaller particles (high mean ξ value of 3.76). Statistical analyses were performed on ξ values to determine whether the different layers exhibited significantly different ξ values. Normality tests (Jarque-Bera test and Shapiro-Wilk test) were performed to check the normality of ξ values in the three layers. Small p values ($p < 0.1$) indicated that the null hypothesis (normality) was rejected, meaning that PSD slope distributions of the three layers were not strictly normal. Nonparametric tests for differences between layers were therefore considered. Two nonparametric tests, Mann-Whitney U test (with the null hypothesis that two groups are taken from populations with equal medians) and Kolmogorov-Smirnov test (with the hypothesis that two groups are taken from populations with equal distributions), were carried out to examine the differences between different layers. Both tests showed very small p values ($p < 0.001$), indicating that PSD slopes in the three layers were from different populations and were significantly different from each other.

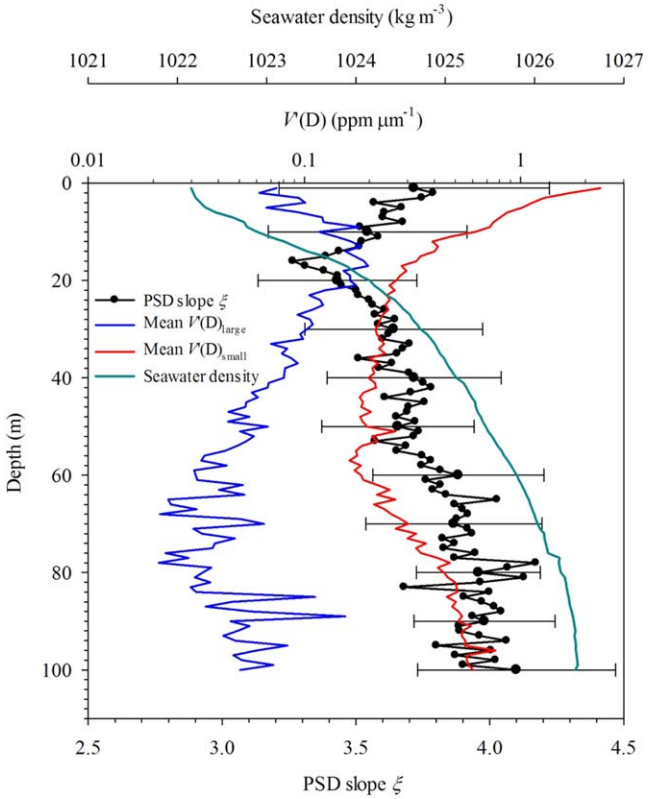

Figure 7. Vertical profiles of the mean PSD slope with SD at 10 m intervals, mean seawater density, mean total volume concentration density at small size class (<10 μm) $V'(D)_{small}$, and mean $V'(D)_{large}$ (>50 μm) from LISST data.

Figure 7 shows the mean vertical profile of the PSD slope using all available data. The mean ξ was higher (~3.6) in the layer above 10 m and reached a minima (~3.3) between 10 and 20 m (where it is associated with the bottom of the mixed layer) and then increased gradually with depth. The mean ξ profile thus showed the same characteristic as the ξ distribution histograms for the three layers (Figure 6), indicating that deep water has higher relative abundance of smaller particles, and thus has higher PSD slopes [*Bader*, 1970]. Figure 7 also shows that volume concentration densities for small particles were higher than for

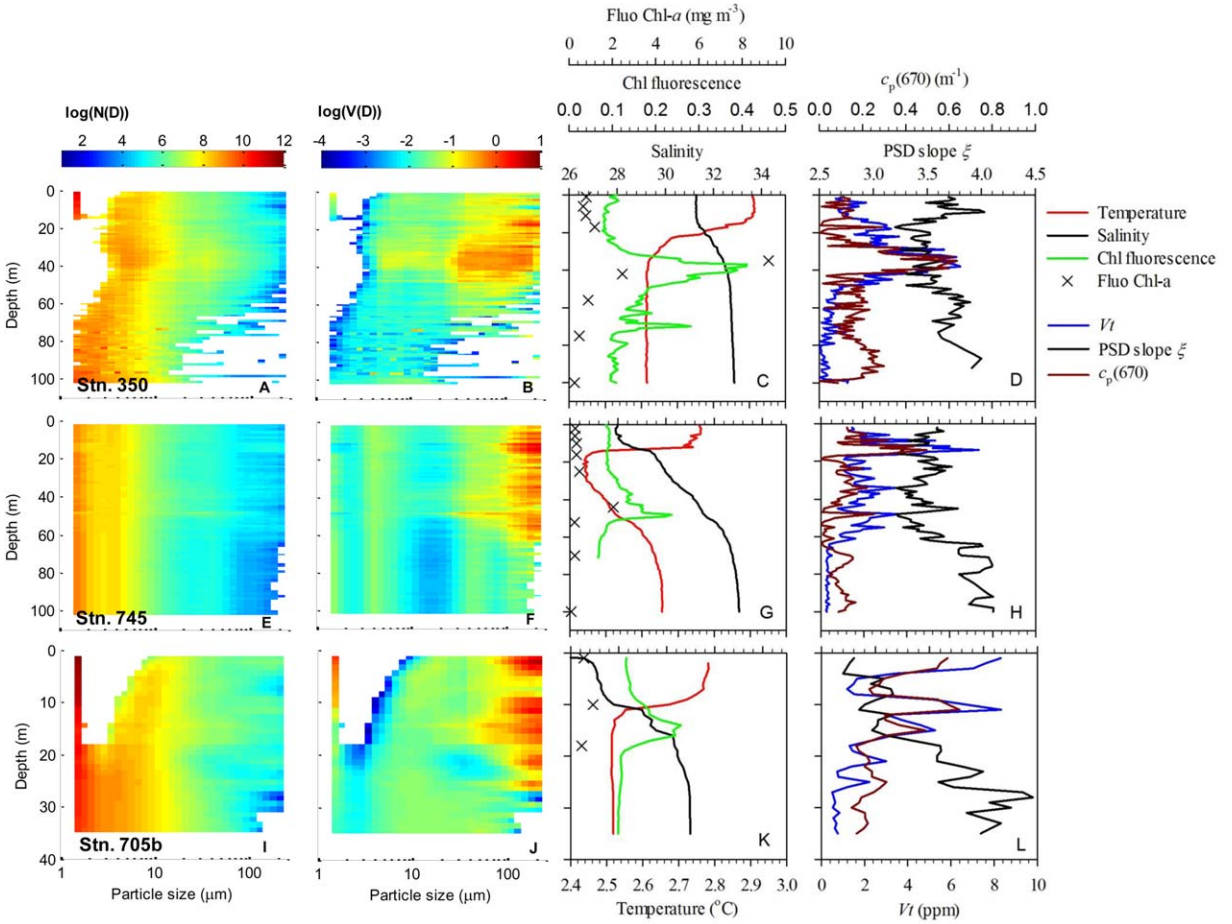

Figure 8. Vertical distributions of (a, e, i) normalized particle number concentration (N(D), m^{-3}), (b, f, g) volume concentration (V(D), ppm), (c, g, k) temperature, salinity, and chlorophyll fluorescence (WetStar) with discrete Chl-*a* values, and (d, h, l) Vt, c_p(670) and PSD slopes at three representative stations (top: Stn. 350; middle: Stn. 745; and bottom: Stn. 705b). Due to the large variation of the magnitudes. Note that N(D) and V(D) are log-transformed due to their wide range of variation. Blank areas in N(D) and V(D) distributions are where no data were collected and therefore were not taken into account when modeling the PSD slope.

large particles down to 20 m, associated with the location of the pycnocline (5–20 m). The accumulation of particles (both small and large) in the pycnocline can occur due to the stable density gradient that separates the upper and lower water layers and hinders vertical transport [*Mann and Lazier*, 2006]. This separation may result in the accumulation and flocculation of the debris of phytoplankton degradation and terrestrial detritus at the base of the mixed layer. Below the pycnocline, the volume concentration of larger particles decreased faster than that of small particles as shown in Figure 7. The gradual increase in small particles volume concentration with depth was possibly related to biogenic material degradation and small particle resuspension near the bottom.

To further illustrate the vertical variability of the PSD, three stations were selected as representative of various Hudson Bay environments along a North-South transect: Stn. 350 in the north, Stn. 745 in the central basin of the Bay, and Stn. 705b in the southwest near the Nelson River estuary (Figure 1). Figure 8 shows the vertical distribution of the N(D) (a, e, i) and V(D) (b, f, j) against particle size classes for the three selected stations. The particle number concentration (N(D)) spanned a wide range (6.30–16.17 $\times$ 10^{11} m^{-3}), and the particle volume concentrations (V(D)) varied from 7.27 $\times$ 10^{-5} to 4.70 ppm with the highest value at the coastal Stn. 705b. Though located at different sites, the three stations showed similar patterns in the vertical distribution of particle number concentrations but with different magnitudes. The vertical profiles at the three stations indicate heterogeneous PSD vertical structure over Hudson Bay. PSD slopes values at Stn. 705b showed the largest vertical variation range ($\sim$1.7) in the upper 40 m layer. All stations showed varying slopes with depth, opposite to the corresponding c_p(670) and Vt profiles. For the three stations, there were

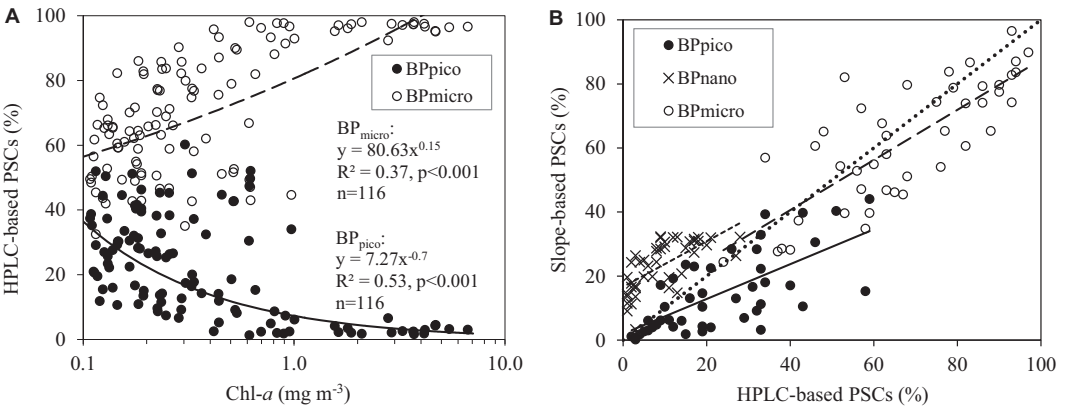

Figure 9. Linear regression between (a) particle size contributions (PSCs) calculated from HPLC data using *Uitz et al*. method and Chl-*a*; and (b) slope-based derived PSCs calculated from the method of *Kostadinov et al*. and HPLC-based PCSs. BP_{pico} ("solid circle," solid line, $y = 0.54x + 1.99$, $R^2 = 0.46$, $p < 0.001$), BP_{nano} ("cross," short dashed line, $y = 0.71x + 16.66$, $R^2 = 0.44$, $p < 0.001$), and BP_{micro} ("open circle," dashed line, $y = 0.78x + 9.25$, $R^2 = 0.61$, $p < 0.001$). The 1:1 diagonal is shown (dotted line) in Figure 9b.

a much larger number of small particles at each depth (Figures 8a, 8e, and 8i). However, when considering the volume occupied by these particles, patches started to appear showing the presence of dominant size class at different depths (Figures 8b, 8f, and 8j).

Stn. 350, located at the entrance of Foxe Basin, is under the influence of arctic water flowing through the Canadian Archipelago. At this deep station (water depth ca. 380 m), the vertical salinity gradient is relatively small due to the absence of a nearby freshwater influence. There was the presence of a large fluorescence peak at 38 m just below the pycnocline, corresponding to the maximum proportion of large particles (small ξ), high $c_p(670)$, and total particle volume (*Vt*). The maximum volume concentration was found at two size classes, i.e., 5–7 μm and 30–200 μm (Figure 8b). In the surface mixed layer, small particles were dominant leading to low *Vt* and $c_p(670)$. There was a patch of large particles (>100 μm) at a depth of 20 m near the bottom of the mixed layer, coupled with a peak in *Vt* and $c_p(670)$. Gravimetric and chemical analyses on suspended matter indicated that the particulate organic matter (POM) contributed 50% and 65% to the TSM in the surface layer and at the DCM depth, respectively, resulting in a good correlation between *Vt* and Chl-*a*. The secondary fluorescence peak observed at 70 m appeared related to the presence of a slightly larger total particle volume with a small decrease of ξ but no effect on $c_p(670)$.

Stn. 745 (180 m depth) is representative of the generally more oligotrophic central portion of Hudson Bay. Postbloom conditions are characterized by low primary production from mainly large cells (>5 μm) [*Ferland et al*., 2011]. In the summer 2010, there was a relatively strong vertical temperature gradient with a shallower mixed layer (15 m). Organic particles contributed more than 70% to the TSM in both the surface layer and at the DCM depth. The depth of maximum chlorophyll fluorescence was 44 m, associated with a small salinity/temperature gradient and a signature on the $c_p(670)$ and *Vt* profiles. There was an increase in the proportion of small particles (larger ξ) just above that feature. Both *Vt* and $c_p(670)$ reached their maxima at the bottom of the surface mixed layer (15 m) associated with an increased number of large particles (>80 μm) (Figure 8f), which probably result from the large particles accumulation on a density discontinuity.

Stn. 705b near the Nelson River estuary in Southwest Hudson Bay has a depth of only 40 m. It is representative of nearshore environments under the influence of freshwater sources. The vertical structure shows a 10 m mixed layer and a DCM at 15 m (Figure 8k). The vertical salinity gradient of 5 reflects the strong stratification resulting from the large freshwater input from the Nelson River and its significant influence on the upper water column. Larger particles (>100 μm) contributed most to total volume at the surface and at two sharp subsurface maxima (10 and 18 m; Figure 8j), leading to characteristic features with small ξ values and strong peaks of both *Vt* and $c_p(670)$. The maximum fluorescence signal was located between the two subsurface particle peaks. The PIM to TSM ratios at the surface and the DCM depth were 73% and 63%, respectively, indicating that most particles masses were inorganic. PIM was the main contributor to particulate attenuation and *Vt* at this station leading to the weak coupling between $c_p(670)$ and Chl-*a*. One interesting feature of the optical profiles is the strong increase in smaller particles near the seabed. This is probably the

result of bottom resuspension of small inorganic particles (<10 μm) leading to a decrease in both $c_p(670)$ and *Vt*.

3.3. Assessment of a Slope-Based Phytoplankton Size Class Method

The PSD shows regional variation in the dominant size classes, which can be partially associated with the presence of different phytoplankton assemblages. A recent intercomparison of particle size class (PSC) methods showed that abundance-based algorithms generally perform well in the remote detection of dominant PSC in oceanic waters [*Brewin et al*., 2010]. Here we did not attempt to determine phytoplankton size classes by inferring size distribution from remote-sensing estimates of particle backscatter [*Kostadinov et al*., 2009]. The availability of LISST data for Hudson Bay provides an opportunity to evaluate this new method against in situ particle size spectra. In order to do so, we used the biomass contribution of pico (BP_{pico}), nano (BP_{nano}), and microplankton (BP_{micro}) derived from HPLC data using the diagnostic pigment analysis (DPA) method [*Uitz et al*., 2006]. This approach has often been used as a benchmark to provide a proxy for size class [*Brewin et al*., 2010].

The analysis was performed on 45 samples where POM:TSM > 65% (estuarine stations are excluded) to constrain the results to reflect oceanic type environments. A significant relationship between HPLC-based and slope-based estimates of the PSCs was found (Figure 9b and relationships therein). This is consistent with the assumption that the PSD slope can be used to quantify the PSCs when biogenic particles dominate [*Kostadinov et al*., 2010, 2012]. Our analysis showed that mean microplankton and picoplankton contributions estimated by the slope method were underestimated (62% and 15% versus 72% and 20%) while the slope-based nanoplankton contribution was overestimated (23% versus 8%) compared to HPLC-based PSCs. Results were consistent over the depth range studied (surface, DCM depths, and other discrete depths). Many factors can explain the discrepancies starting with the intrinsic inaccuracy of the diagnostic pigment analysis (DPA) method which is directly affected by the precision of HPLC analysis, i.e., 21.5% for pigments other than Chl-*a* [*Claustre et al*., 2004]. Second, one assumption of the DPA is that specific pigments are representative of certain size classes whereas some degree of variability exists in natural assemblages [*Vidussi et al*., 2001; *Uitz et al*., 2006]. Also, as shown in Figure 3, the power-law function did not provide a perfect estimation of true particle size spectra. Microplankton in (20–80 μm) was generally overestimated but underestimated in (80–200 μm). Nanoplankton in (6–12 μm) was underestimated but overestimated in (12–20 μm). Therefore, underestimation and overestimation both existed for each size group leading to decrease the bias for the whole range of a group. The slope-based picoplankton proportion was calculated using only the power-law fit to the smaller sizes using ξ values, thus uncertainties existed in this size range and had effect on the micro and nanoplankton proportions as well. An additional source of error may be the fact that the particle size range (6.14–196 μm) used to calculate ξ is different than the slope-based model range (0.5–200 μm). Different total particle size ranges would change, to a certain extent, the estimated proportions of each phytoplankton functional types [*Kostadinov et al*., 2009, 2010, 2012].

Overall, despite of uncertainties in the slope-based PSCs, the agreement between slope-based PSCs and HPLC-based PSCs is considered relatively good, supporting the use of remote sensing to infer particle size distribution in offshore waters of Hudson Bay. One important observation from the in situ samples is the apparent dominance of microplankton (62%, Figure 9a) at low Chl-*a* concentrations. This can be explained by the presence of fucoxanthin in small cells such as prymnesiophytes, chrysophytes, and small flagellates in addition to its typical occurrence in diatoms [*Hirata et al*., 2011]. Indeed, protist cell counts identified that these small phytoplankton cells dominated suspended assemblages at offshore stations in 2010.

4. Conclusions

Particle size distribution measurements in Hudson Bay showed significant regional and vertical variability both in the particle concentrations and slopes. A strong association of larger particles with the base of the mixed layer was observed, probably resulting from the particles accumulation on a density discontinuity. The PSD-derived PSCs were found to be consistent with HPLC-derived PSCs in offshore waters, lending support to the retrieval of PSCs from remote sensing even though the power-law model has limitations in capturing spectral size complexities. To conclude, this study provides baseline knowledge on the PSD properties and variability with regard to the nature of suspended assemblages in Hudson Bay waters. These results apply to the summer period, characterized by very low phytoplankton biomasses [*Xi et al*., 2013].

Further study of the seasonal variability associated with changes in phytoplankton abundance and composition in this high latitude system is warranted. In addition, future research will focus on optical properties of marine particles in Hudson Bay and remote sensing applications, including backscattering to scattering ratio of particles and relationships to their biogeochemical composition and applications of the PSD.

Notation

DCM	deep chlorophyll maximum.
c_p	particulate beam attenuation coefficient measured by LISST, m^{-1}.
Fluo. Chl-*a*	chlorophyll-*a* concentration measured by fluorescence method, mg m^{-3}.
HPLC Chl-*a*	chlorophyll-*a* concentration measured by HPLC, mg m^{-3}.
Chl fluorescence	chlorophyll fluorescence from WetStar.
ξ	Junge slope of the particle size distribution (PSD).
λ	wavelength, nm.
MLD	mixed layer depth, m.
$N(D)$	particle number concentration at size class D, m^{-3}.
$N'(D)$	particle number density at size class D, $m^{-3}\ \mu m^{-1}$.
$N'(D)_{small}$	total particle number density at small size classes ($<10\ \mu m$), $m^{-3}\ \mu m^{-1}$.
$N'(D)_{medium}$	total particle number density at medium size classes (10–50 μm), $m^{-3}\ \mu m^{-1}$.
$N'(D)_{large}$	total particle number density at large size classes ($>50\ \mu m$), $m^{-3}\ \mu m^{-1}$.
PIM	particulate inorganic matter, g m^{-3}.
POM	particulate organic matter, g m^{-3}.
PSD	particle size distribution.
TSM	total suspended matter, g m^{-3}.
$V(D)$	volume concentration at size class D, ppm.
$V'(D)$	volume concentration density at size class D, ppm μm^{-1}.
$V'(D)_{small}$	total volume concentration density at small size classes ($<10\ \mu m$), ppm μm^{-1}.
$V'(D)_{medium}$	total volume concentration density at medium size classes (10–50 μm), ppm μm^{-1}.
$V'(D)_{large}$	total volume concentration density at large size classes ($>50\ \mu m$), ppm μm^{-1}.
Vt	total volume concentration within range of 6.14–196 μm.
PSC	phytoplankton size-class.
BP_{pico}	biomass proportion of picoplankton ($<2\ \mu m$).
BP_{nano}	biomass proportion of nanoplankton (2–20 μm).
BP_{micro}	biomass proportion of microplankton (20–200 μm).

Acknowledgments

This work was made possible with the support of the Natural Sciences and Engineering Research Council of Canada (NSERC), the Department of Fisheries and Oceans Canada, and the Canadian Space Agency. We are grateful to the crew of the NGCC Amundsen during the 2010 ArcticNet expedition for their dedication supporting science activities. We acknowledge the important contribution of Michel Gosselin who provided the size-fractionated chlorophyll measurements and Mehmet Yayla who helped to determine the PSCs from HPLC measurements. Finally, we acknowledge the work of Emmanuel Boss and another anonymous referee who provided valuable comments on the manuscript.

References

Agrawal, Y. (2005), The optical volume scattering function: Temporal and vertical variability in the water column off the New Jersey coast, *Limnol. Oceanogr. Methods*, *50*, 1787–1794.

Agrawal, Y., and H. Pottsmith (2000), Instruments for particle size and settling velocity observation in sediment transport, *Mar. Geol.*, *168*, 89–114, doi:10.1016/S0025-3227(00)00044-X.

Agrawal, Y., and P. Traykovski (2001), Particles in the bottom boundary layer: Concentration and size dynamics through events, *J. Geophys. Res.*, *106*(C5), 9533–9542, doi:10.1029/2000JC900160.

Agrawal, Y., A. Whitmire, O. Mikkelsen, and H. Pottsmith (2008), Light scattering by random shaped particles and consequences on measuring suspended sediments by laser diffraction, *J. Geophys. Res.*, *113*, C04023, doi:10.1029/2007JC004403.

Ahn, J. H. (2012), Size distribution and settling velocities of suspended particles in a tidal embayment, *Water Res.*, *46*, 3219–3228, doi: 10.1016/j.watres.2012.03.038.

Andrews, S., D. Nover, and S. G. Schladow (2010), Using laser diffraction data to obtain accurate particle size distributions: The role of particle composition, *Limnol. Oceanogr. Methods*, *8*, 507–526, doi:10.4319/lom.2010.8.507.

Andrews, S. W., D. M. Nover, K. E. Reardon, J. E. Reuter, and S. G. Schladow (2011), The influence of ambient light intensity on in situ laser diffractometers, *Water Resour. Res.*, *47*, W06509, doi:10.1029/2010WR009841.

Aurin, D., H. M. Dierssen, M. S. Twardowski, and C. S. Roesler (2010), Optical complexity in Long Island Sound and implications for coastal ocean color remote sensing, *J. Geophys. Res.*, *115*, C07011, doi:10.1029/2009JC005837.

Bader, H. (1970), The hyperbolic distribution of particle sizes, *J. Geophys. Res.*, *75*(15), 2822–2830, doi:10.1029/JC075i015p02822.

Boss, E., and W. S. Pegau (2001), The relationship of light scattering at an angle in the backward direction to the backscattering coefficient, *Appl. Opt.*, *40*, 5503–5507, doi:10.1364/AO.40.005503.

Boss, E., W. S. Pegau, W. D. Gardner, R. V. Zaneveld, A. H. Barnard, M. S. Twardowski, G. C. Chang, and T. D. Dickey (2001a), Spectral particulate attenuation and particle size distribution in the bottom boundary layer of a continental shelf, *J. Geophys. Res.*, *106*(C5), 9509–9516, doi:10.1029/2000JC900077.

Boss, E., M. S. Twardowski, and S. Herring (2001b), Shape of the particulate beam attenuation spectrum and its inversion to obtain the shape of the particulate size distribution, *Appl. Opt.*, *40*, 4885–4893, doi:10.1364/AO.40.004885.
Brewin, R. J. W., S. Sathyendranath, T. Hirata, S. J. Lavender, R. Barciela, and N. J. Hardman-Mountford (2010), A three-component model of phytoplankton size class from satellite remote sensing, *Ecol. Modell.*, *221*(11), 1472–1483, doi:10.1016/j.ecolmodel.2010.02.014.
Bricaud, A., A. Morel, and L. Prieur (1981), Absorption by dissolved organic matter of the sea (yellow substance) in the UV and visible domains, *Limnol. Oceanogr.*, *26*, 43–53, doi:10.4319/lo.1981.26.1.0043.
Bricaud, A., H. Claustre, J. Ras, and K. Oubelkheir (2004), Natural variability of phytoplanktonic absorption in oceanic waters: Influence of the size structure of algal populations, *J. Geophys. Res.*, *109*, C11010, doi:10.1029/2004JC002419.
Buonassissi, C. J., and H. M. Dierssen (2010), A regional comparison of particle size distributions and the power law approximation in oceanic and estuarine surface waters, *J. Geophys. Res.*, *115*, C10028, doi:10.1029/2010JC006256.
Claustre, H., et al. (2004), An intercomparison of HPLC phytoplankton methods using in situ samples: Application to remote sensing and database activities, *Mar. Chem.*, *85*(1–2), 41–61.
Dall'Olmo, G., T. K. Westberry, M. J. Behrenfeld, E. Boss, and W. H. Slade (2009), Significant contribution of large particles to optical backscattering in the open ocean, *Biogeosciences*, *6*, 947–967, doi:10.5194/bg-6-947-2009.
Darecki, M., S. Kaczmarek, and J. Olsweski (2005), SeaWiFS ocean colour chlorophyll algorithms for the southern Baltic sea, *Int. J. Remote Sens.*, *26*, 247–260, doi:10.1080/01431160410001720298.
Falkowski, P. G., E. A. Laws, R. T. Barber, and J. W. Murray (2003), Phytoplankton and their role in primary, new, and export production, in *Ocean Biogeochemistry: The Role of the Ocean Carbon Cycle in Global Change*, edited by M. J. R. Fasham, pp. 99–121, Springer, Berlin.
Falkowski, P. G., R. T. Barber, and V. Smetacek (1998), Biogeochemical controls and feedbacks on ocean primary production, *Science*, *281*, 200–206, doi:10.1126/science.281.5374.200.
Ferland, J., M. Gosselin, and M. Starr (2011), Environmental control of summer primary production in the Hudson Bay system: The role of Stratification, *J. Mar. Syst.*, *88*, 385–400, doi:10.1016/j.jmarsys.2011.03.015.
Hirata, T., et al. (2011), Synoptic relationships between surface chlorophyll-a and diagnostic pigments specific to phytoplankton functional types, *Biogeosciences*, *8*, 311–327, doi:10.5194/bg-8–311-2011.
Hood, R. R., et al. (2006), Pelagic functional group modeling: Progress, challenges and prospects, *Deep Sea Res., Part II*, *53*, 459–512.
Jonasz, M. (1983), Particle size distribution in the Baltic, *Tellus, Ser. B*, *35*, 346–358, doi:10.1111/j.1600-0889.1983.tb00039.x.
Jonasz, M., and G. Fournier (2007), *Light Scattering by Particles in Water: Theoretical and Experimental Foundations*, Academic, London.
Karageorgis, A. P., D. Georgopoulos, T. D. Kanellopoulos, O. A. Mikkelsen, K. Pagou, H. Kontoyiannis, A. Paylidou, and Ch. Anagnostou (2012), Spatial and seasonal variability of particulate matter optical and size properties in the Eastern Mediterranean Sea, *J. Mar. Syst.*, *105–108*, 123–134.
Karp-Boss, L., L. Azevedo, and E. Boss (2007), LISST-100 measurements of phytoplankton size distribution: Evaluation of the effects of cell shape, *Limnol. Oceanogr. Methods*, *5*, 396–406.
Kiefer, D. A., and J. Berwald (1992), A random encounter model for the microbial planktonic community, *Limnol. Oceanogr.*, *37*, 457–467.
Kostadinov, T. S., D. A. Siegel, and S. Maritorena (2010), Global variability of phytoplankton functional types from space: Assessment via the particle size distribution, *Biogeosciences*, *7*, 3239–3257, doi:10.5194/bg-7-3239-2010.
Kostadinov, T. S., D. A. Siegel, and S. Maritorena (2009), Retrieval of the particle size distribution from satellite ocean color observations, *J. Geophys. Res.*, *114*, C09015, doi:10.1029/2009JC005303.
Kostadinov, T. S., D. A. Siegel, S. Maritorena, and N. Guillocheau (2012), Optical assessment of particle size and composition in the Santa Barbara Channel, California, *Appl. Opt.*, *51*(6), 3171–3189, doi:10.1029/2009JC005303.
LISST-100X Particle Size Analyzer (2013), *User's Manual Version 5.0*, Sequoia Sci., Inc., Bellevue, Wash.
Loisel, H., J.-M. Nicolas, A. Sciandra, D. Stramski, and A. Poteau (2006), Spectral dependency of optical backscattering bymarine particles from satellite remote sensing of the global ocean, *J. Geophys. Res.*, *111*, C09024, doi:10.1029/2005JC003367.
Mann, K. H., and J. R. N. Lazier (2006), *Dynamics of Marine Ecosystems: Biological-Physical Interactions in the Oceans*, Blackwell, Oxford, U. K.
Marrari, M., C. Hu, and K. Daly (2006), Validation of SeaWiFS chlorophyll a concentrations in the Southern Ocean: A revisit, *Remote Sens. Environ.*, *105*, 367–375.
Mikkelsen, O., and M. Pejrup (2001), The use of a LISST-100 laser particle sizer for in-situ estimates of floc size, density and settling velocity, *Geo Mar. Lett.*, *20*, 187–195.
Mikkelsen, O. A., T. G. Milligan, P. S. Hill, R. J. Chant, C. F. Jago, S. E. Jones, V. Krivtsov, and G. Mitchelson-Jacob (2008), The influence of schlieren on in situ optical measurements used for particle characterization, *Limnol. Oceanogr. Methods*, *6*, 133–143.
Morel, A. (1973), Light scattering by seawater, experimental results and theoretical approach (Diffusion de la lumière par les eaux de mer; résultats expérimentaux et approche théorique; in French), in *Optics of the Sea, Interface and In-Water Transmission and Imaging*, AGARD Lecture Series No. 61, Published in August 1973, pp. 3.1.1–3.1.76.
Mustapha, S. B., S. Bélanger, and P. Larouche (2012), Evaluation of ocean color algorithms in the southeastern Beaufort Sea, Canadian Arctic: New parametrization using SeaWiFS, MODIS and MERIS spectral bands, *Can. J. Remote Sens.*, *38*(5), 1–22.
Neukermans, G., H. Loisel, X. Mériaux, R. Astoreca, and D. McKee (2012), In situ variability of mass-specific beam attenuation and backscattering of marine particles with respect to particle size, density, and composition, *Limnol. Oceanogr. Methods*, *57*, 124–144.
Platt, T., and K. Denman (1978), The structure of the pelagic marine ecosystem, *Rapp. P. V. Reun. Cons. Int. Explor. Mer.*, *173*, 60–65.
Reynolds, R. A., D. Stramski, V. M. Wright, and S. B. Woźniak (2010), Measurements and characterization of particle size distributions in coastal waters, *J. Geophys. Res.*, *115*, C08024, doi:10.1029/2009JC005930.
Risovic, D. (1993), Two-component model of sea particle size distribution, *Deep Sea Res., Part I*, *40*, 1459–1473.
Sheldon, R. W., A. Prakash, and W. H. Sutcliffe Jr. (1972), The size distribution of particles in the ocean, *Limnol. Oceanogr.*, *17*, 327–340.
Stramski, D., A. Bricaud, and A. Morel (2001), Modelling the inherent optical properties of the ocean based on the detailed composition of the planktonic community, *Appl. Opt.*, *40*, 2929–2945, doi:10.1364/AO.40.002929.
Stramski, D., and D. Kiefer (1991), Light scattering by microorganisms in the open ocean, *Prog. Oceanogr.*, *28*, 343–383, doi:10.1016/0079-6611(91)90032-H.
Sullivan, J. M., M. S. Twardowski, P. L. Donaghay, and S. A. Freeman (2005), Use of optical scattering to discriminate particle types in coastal waters, *Appl. Opt.*, *44*, 1667–1680, doi:10.1364/AO.44.001667.
Twardowski, M. S., E. Boss, J. B. MacDonald, W. S. Pegau, A. H. Barnard, and J. R. V. Zaneveld (2001), A model for estimating bulk refractive index from optical backscattering ratio and the implications for understanding particle composition in case I and case II waters, *J. Geophys. Res.*, *106*(C7), 14,129–14,142, doi:10.1029/2000JC000404.

Uitz, J., H. Claustre, A. Morel, and S. B. Hooker (2006), Vertical distribution of phytoplankton communities in open ocean: An assessment based on surface chlorophyll, *J. Geophys. Res.*, *111*, C08005, doi:10.1029/2005JC003207.

Van Heukelem, L., and C. S. Thomas (2005), The HPL method in the second SeaWiFS HPLC analysis round-robin experiment (SeaHARRE-2), *NASA TM/2005–212785*, pp. 86–92, NASA Goddard Space Flight Cent., Greenbelt, Md.

Vidondo, B., Y. T. Prairiej, M. Blanco, and C. M. Duarte (1997), Some aspects of the analysis of size spectra in aquatic ecology, *Limnol. Oceanogr.*, *42*, 184–192, doi:10.4319/lo.1997.42.1.0184.

Vidussi, F., H. Claustre, B. B. Manca, A. Luchetta, and J. C. Marty (2001), Phytoplankton pigment distribution in relation to upper thermocline circulation in the eastern Mediterranean Sea during winter, *J. Geophys. Res.*, *106*(C9), 19,939–19,956, doi:10.1029/1999JC000308.

Xi, H., P. Larouche, S. Tang, and C. Michel (2013), Seasonal variability of light absorption properties and water optical constituents in Hudson Bay, Canada, *J. Geophys. Res.*, *118*, 3087–3102, doi:10.1002/jgrc.20237.

Yentsch, C., and D. W. Menzel (1963), A method for the determination of phytoplankton chlorophyll and phaeophytin by fluorescence, *Deep Sea Res., Oceanogr. Abstr.*, *10*, 221–231.